Materials and Structures
DOI 10.1617/s11527-012-9860-z

ORIGINAL ARTICLE

Optical method for measuring slow crack growth in cementitious materials

W. Cai · J. Bisschop

Received: 30 March 2011 / Accepted: 10 April 2012

Abstract The double-torsion (DT) test is commonly used to calculate slow or subcritical crack velocities in (quasi-)brittle engineering materials directly from the measured load relaxation of notched DT-specimens. In cementitious materials a significant part of the recorded load relaxation in the DT-test may be due to specimen creep deformation, and this would then lead to overestimated crack velocities. In this paper we describe a method to optically measure slow crack growth in cementitious materials by carrying out DT-tests under the optical microscope or inside the environmental SEM. Crack tip detection is facilitated by digital image correlation of the time-lapse microscope recordings. DT-tests at 10 % relative humidity in hardened cement paste (with w/c-ratio of 0.4, 0.5 and 0.6) showed that optically measured crack velocities were significantly lower than those calculated from the DT-specimen relaxation. In many experiments the subcritical crack growth rapidly stopped, while an ongoing specimen load relaxation was recorded. At 90 % relative humidity, load-relaxation in the DT-test was much stronger than at 10 % relative humidity, because subcritical cracking and creep-induced relaxation both increase with moisture content.

W. Cai (✉) · J. Bisschop
Institute for Building Materials, ETH-Zürich,
Schafmattstrasse 6, 8093 Zürich, Switzerland
e-mail: wcai@ethz.ch

Published online: 24 April 2012

Keywords Subcritical cracking · Microcracking · Crack detection · Cement paste · Creep

Mathematical Subject Classification 74A45 · 74C10 · 74R10

1 Introduction

The life-time of concrete structures under high sustained loads is not only affected by chemical interactions with the environment, but also by intrinsic mechanical processes that may reduce the long-term strength of concrete. It is well known that the static strength of cementitious materials depends on loading rate: slower loading generally results in a lower measured strength [1–3]. This is caused by (i) time-dependent fracture and by (ii) creep of cementitious materials [4, 5]. The mechanism of time-dependent fracture in cementitious materials according to Bažant et al. [6] is a thermally activated process in the stressed crack tip. This is essentially similar to the phenomenon of *subcritical cracking* that is well known from other materials such as glass, ceramics, and rocks [7–9]. Subcritical cracking occurs at a stress intensity factor (K) below the critical fracture toughness (K_{IC}) and is strongly influenced by the relative humidity (RH) of the environment or in the crack tip [7–9].

Basic creep may have positive or negative effects on the long-term strength of cementitious materials.

Basic creep causes consolidation of the material under compression that leads to increased strength upon reloading [10–13], and creep may lower crack tip stresses by crack tip 'blunting' [1, 2]. On the contrary, basic creep may contribute to failure if failure is governed by a maximum strain criterion [1]. It has also been postulated that creep is a mechanism of subcritical cracking in cementitious materials [14].

For life-time analyses of concrete under sustained load it is important to understand the respective effects of creep and subcritical cracking on long-term strength. In pure brittle materials such as glass and certain rock types, the phenomenon of subcritical (i.e., time-dependent or environment-driven) cracking is well defined and can be measured relatively easily in, for example, the DT-test [7]. In cementitious materials this is not the case because of fracture-creep interactions that are likely to occur under slow or sustained loading. There have been a number of studies aimed at measuring subcritical cracking in cementitious materials using the DT-test under the assumption that measured specimen relaxation was primarily due to crack propagation [15–19]. If load-relaxation also occurs due to creep deformation of DT specimens as observed by Wecharatana and Shah [20] and in this study, then subcritical crack velocities calculated directly from measured specimen load-relaxation are overestimates.

Of particular interest is to measure the effect of relative humidity or moisture content on subcritical cracking in cementitious materials. It is well known that increasing moisture content lowers the fracture energy/toughness or time-to-failure of cementitious materials [11, 21–25]. Studies showed that cementitious materials were more susceptible to subcritical cracking at higher relative humidity in the DT-test [15, 17], but possible contributions of creep in the measured specimen load-relaxation were not addressed in these studies. The importance of specimen creep in the DT-test is expected to become larger at higher relative humidity, because creep strain increases with moisture content [26–28].

In this paper an experimental method is described to measure subcritical crack velocity optically at controlled relative humidity inside the environmental scanning electron microscope (ESEM) or under a stereomicroscope. Crack growth processes have been studied before in situ inside the SEM, even under partly wet conditions [29–33], but in none of the previous studies subcritical crack velocities have been reported. The optically measured subcritical crack velocities reported in this paper show the importance of creep-induced relaxation in DT specimens of cementitious materials.

2 Methods

2.1 Loading system

In this study the DT-test was employed to study subcritical cracking in hardened Portland cement paste. The DT-test is a three-point bending test on one end of a notched rectangular plate-shaped specimen (Fig. 1a). An advantage of the DT-test is that the stress intensity factor is independent of the crack length in the middle part of the DT-specimen [34]. The DT micro-loading device constructed for this study consists of a loading stage, a Peltier cooling/heating stage, a control unit and a data acquisition unit (Fig. 1b). The loading stage consists of a stepper motor mounted together with a zero backlash spur gear head, a linear variable displacement transducer (LVDT), a load cell (accuracy ±0.1 N) and a micro-transmission system. The DT microstage was specifically designed to function inside the ESEM vacuum chamber. The set-up was also used at ambient conditions under an optical microscope. The relaxation of the loading stage was examined by using stiff specimens (e.g., brass) and was very small at the load level of the DT-tests (i.e., within the error range of the load cell). The loading stage relaxation was subtracted from the total measured relaxation to obtain the specimen load relaxation.

2.2 Materials and specimen preparation

All specimens were prepared from 63 μm sieved Portland cement (CEM I 52.5R) with added water-cement (w/c) ratio's of 0.4, 0.5 or 0.6. The cement pastes were stirred in a Hobart mixer for 5 min, followed by 5 min of high-speed stirring using a mixing spoon attached to a drilling machine. The specimens were cast in $65 \times 25 \times 10$ mm^3 brass moulds. A brass piece with an inverse T-shaped cross section was fixed on the bottom of the mould to form a 1 mm wide × 3 mm deep guiding groove in each specimen (Fig. 1a). The moulds were briefly vibrated on a table vibrator, sealed with plastic foil and stored in a conditioning room at 100 % RH at 20 °C. After 1 day the specimens were

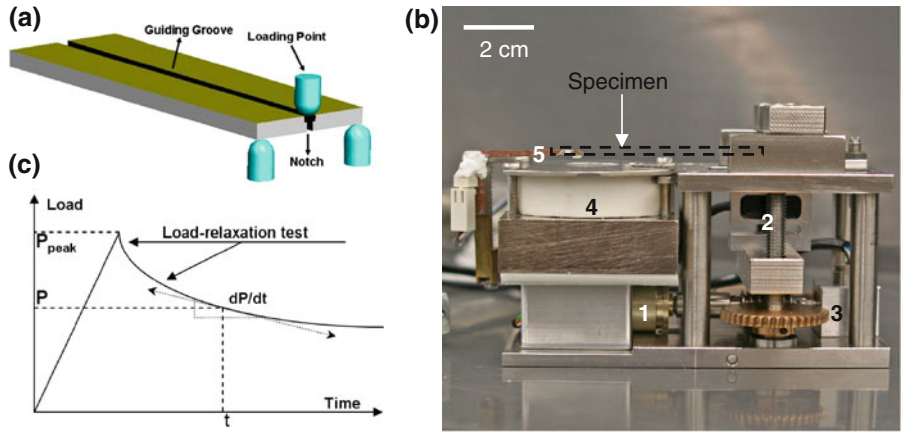

Fig. 1 The double-torsion test: **a** loading configuration of the DT-specimen; **b** the loading stage: *1* stepper motor, *2* load cell, *3* LVDT gauge, *4* cooling stage, *5* T-sensor; **c** schematic load relaxation curve in a DT-test

removed from the moulds and placed in lime water for 9–10 months. DT-specimens of 60 × 25 × 1.7 mm^3 were prepared by coarse grinding on grit-120 sand paper, followed by fine-grinding on grit-1000 sand paper. Before thinning, a 10 mm deep × 0.45 mm wide notch was cut by a diamond saw in one end of the specimens (Fig. 1a). The specimen thickness was kept below 2 mm to avoid desiccation cracking that otherwise may occur upon equilibrating or testing the specimens at low relative humidity (e.g. 10 % RH) [35, 36]. No desiccation microcracks were observed in any of the tested samples. Additional unnotched specimens of 28 × 4 × 2 mm^3 were prepared for beam bending tests in the DT set-up to measure creep-induced relaxation of the cement pastes. The age of all specimens at the time of testing varied between 9 and 10 months. It was assumed that the variation in age between 9 and 10 months had little effect on the fracture behavior.

Reference experiments were carried out on samples of single-crystal calcite ($CaCO_3$) that does not creep at room temperature and fractures straight along its cleavage planes. Specimens of 30 × 10 × 1 mm^3 were cut with the 1 × 30 mm^2 sides parallel to a cleavage plane, with all the other sides normal to this plane and thus miscut with respect to the calcite rhomb. The specimens were prepared by Photox Optical Systems Ltd. from mined calcite crystals. The 10 × 30 mm^2 surfaces were optically polished. A start cleavage crack (notch) about 3 mm in length was made on one end of the specimen by razor blade scratching.

2.3 Load-relaxation tests

In this study specimen load relaxation in the double torsion test was measured under constant displacement conditions. Before each test, the specimen was moisture-equilibrated (at the relative humidity applied in the DT-test) in a climate chamber (Vötsch VC4060) for 5–7 days until its weight stabilized. After placing the sample in the loading stage, it was again equilibrated at the intended relative humidity and temperature conditions of the test until the force reading was constant. The specimen was then loaded at a speed of 1.5 μm/min until a major crack was initiated at the peak load. The crack was controlled to propagate step by step until it extended into the middle region of the specimen, where the stress intensity factor is expected to be independent of the crack length [33]. The sample was loaded one more time at 1.5 μm/min to the peak load after which the displacement of the loading points was held constant. Specimen load relaxation was recorded for about 30 min during which the crack propagated over tens to hundreds of micrometers. Up to 3 relaxation tests could be performed in one specimen.

The temperature of the DT-specimen was controlled by letting it rest on an aluminum table connected to the cooling stage (not shown in Fig. 1b). A temperature sensor was placed on top of the DT-specimen to monitor the specimen temperature. All DT-tests at 10 % RH were carried out in the ESEM at 2.4 Torr and 24 °C. Some DT-tests at 90 % RH (20 Torr, 24 °C) were also carried out in the

ESEM-chamber, but imaging was then not possible since the pressure should be below 5 Torr for recording ESEM images with reasonable quality. Imaging conditions at 90 % RH have to be achieved by setting the specimen temperature to below 5 °C. However, this is very difficult because the specimen was not making a perfect contact with the cooling table during the DT-torsion test and the vacuum in the ESEM chamber impedes good heat conduction. DT-tests at 90 % RH were therefore primarily carried out under an optical stereomicroscope in a conditioning room at 65 % RH, 20 °C with the specimen cooled down to 15 °C.

2.4 Crack velocity calculated from load relaxation

In brittle, non-creeping materials subcritical crack velocities can be calculated from the measured load-relaxation using the following equation [34]:

$$v = \mathrm{d}a/\mathrm{d}t = -a_i\left(P_i/P^2\right)(\mathrm{d}P/\mathrm{d}t) \quad (1)$$

where P is the load, a_i is the initial or final crack length, P_i is the initial or final load with respect to a_i, and t is the time (Fig. 1c). Since hardened cement paste specimens in this study showed significant creep-induced load-relaxation, the velocities calculated by using this equation are too high. The stress intensity factor was calculated according to [34]:

$$K = PS_m\left[3(1+v)/wd_nd^3\psi\right]^{0.5} \quad (2)$$

In which, S_m is the moment arm of the load, v is the Poisson's ratio, w is specimen width, d is specimen thickness, d_n is the thickness above the guiding groove and ψ is a correction factor for thick specimens given by $\psi = 1\text{-}0.6302(2d/w) + 1.20(2d/w)\mathrm{EXP}(-\pi w/2d)$ [37]. The results are plotted in the traditional K–v diagram.

2.5 Optical measurement of crack velocity

During each DT-test as many as possible microscope images were taken for the specimen region containing the crack tip. Note that the crack front is curved in DT specimens [9], and the observation for the crack tip was made on the tension side of the specimen. In a few high quality ESEM image series the crack tip position could be directly located. In most cases digital image correlation (DIC) of the microscope recording was used to determine crack tip locations. DIC is a technique to measure 2D displacement or strain fields from time-laps image series [38, 39]. This method calculates the correlation between different groups of pixels, so-called subsets, in the first undeformed image and following deformed images. By tracking these subsets in each successive image, the maximum correlation can be found to obtain the relative displacement for each subset center. The displacement field can be differentiated to derive the principle strain field. The width of the cracks in the DIC strain fields depends on the chosen strain window size that defines the number of adjacent subsets which are used to calculate the average strain over a certain region. A smaller strain window produces thinner 'cracks', but increases noise and number of miscalculations in the strain image. The crack opening strain (COS) used in this study (in Fig. 6) is an approximate measure for crack opening, because it is calculated using a strain window (size of about 18 μm), which is larger than the actual crack width near the tip (1–2 μm). VIC 2D software from *Correlated Solutions* was used in this study to perform the DIC analysis.

The resolution of DIC in this study was not high enough to observe elastic or creep deformations in the specimens, or the fracture process zone, but the technique is well suited for detecting cracks. The measured crack tip positions from DIC are probably not the very end of cracks. Nevertheless DIC allows to unambiguously record and track a near crack tip position (i.e., a border line of two strain colors), the velocity of which is expected to be proportional to the real crack tip velocity. Crack tip detection by DIC can be done both by comparing two successive images (=incremental strain) or by comparing an image to the initial, undeformed image (=total strain). As aforementioned, ESEM imaging was only possible during the DT-tests at 10 % RH. Most DT-tests at 90 % RH were therefore carried out under an optical stereomicroscope. However, the success rate of recording crack tip propagation rates using optical microscopy was limited because the tip part of subcritical crack could not be seen at the highest magnification. The position of the crack tip therefore needed to be estimated and in many cases was not properly captured in time-lapse images required for accurate DIC.

Under the optical microscope at low magnification, the velocity was calculated by dividing the travelled distance of the crack tip (measured from the DIC strain fields) by the recorded time of two successive images. ESEM images are acquired through line-by-line scanning, meaning that a certain amount of time is required

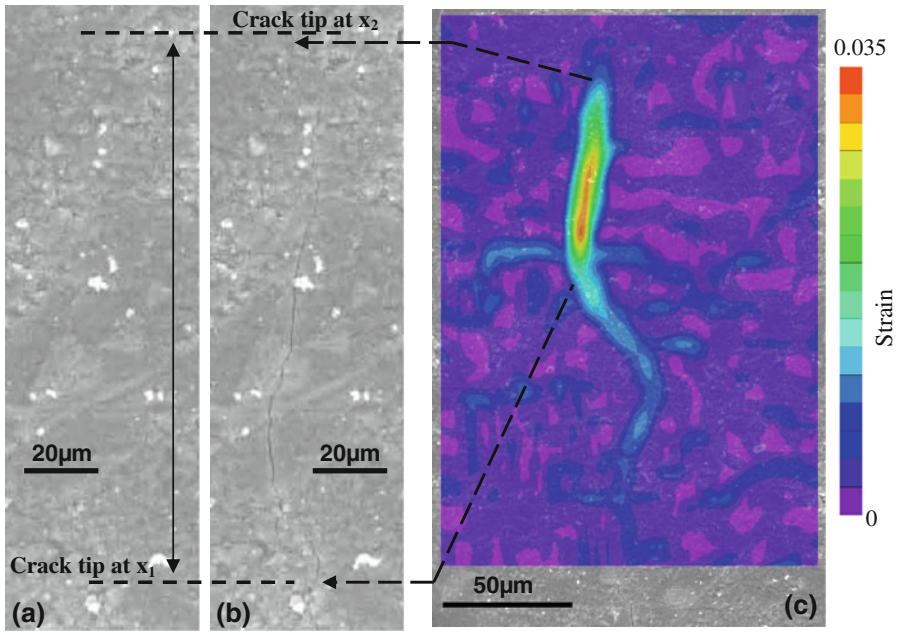

Fig. 2 Principle of crack velocity measurement in SEM (see text for explanation): **a** image at time t_1; **b** image at time t_2; **c** digital image correlation result showing the principal tensile (incremental) strain field around the incremental crack. Image scanning direction is from *left* to *right* and from *top* to *bottom*. These are ESEM-GSE images

to obtain the image. The principle of measuring crack velocity from ESEM images is shown in Fig. 2. At time t_1, the first image scan started and the time to reach the crack tip was Δt_1, at t_2 the second scan started and the crack tip was reached after Δt_2. The total time between two crack tip locations was $\Delta t = (t_2 + \Delta t_2) - (t_1 + \Delta t_1)$. Δt_1 and Δt_2 were determined by measuring the distance in pixels from the image top to the crack tip and multiplying this distance by the line scan time. The crack tip velocity obtained is this way is an average minimum velocity when the crack moves in a discontinuous manner. The highest crack velocity that can be obtained in ESEM experiments depends on the displacement rate of the ESEM sample/stage holder (in case crack tip moves out of the initial image frame), and on the chosen image acquisition rate (i.e., line scanning speed). In this study the highest recorded crack tip velocity using SEM was approximately 0.6 mm/s. Under the optical microscope that maximum measurable velocity is expected to be much higher and depends on the camera shutter speed.

3 Results and discussion

3.1 Double-torsion tests on calcite

As a reference to hardened cement paste, DT-tests were carried out on specimens of single crystal (Iceland Spar) calcite. In these tests subcritical crack velocities were calculated from load-relaxation (Eq. 1) and optically from ESEM images. Calcite does not exhibit significant creep at room temperature (e.g. Bažant et al. [40]) and breaks straight along cleavage planes meaning that no guiding groove in the specimens is required. The subcritical crack is easily detected on SEM images as a white line using the SE-detector (Fig. 3). The crack-tip is defined as the point where the white line changes to black (arrow in Fig. 3). Although this might be not the very crack tip, it is expected to be a point close to the crack tip that can be tracked in time with an accuracy of ±2 μm. The total distance travelled by the crack tip in a single relaxation run was between 50 and 200 μm. There is a good general agreement between the crack velocities obtained from the load-relaxation and those from ESEM images. This shows that there is no significant relaxation in the micro-loading stage and that for non-creeping materials Eq. 1 provides good velocity calculations. Note that these calcite experiments were carried out at 1 % RH to improve ESEM image quality and facilitate crack tip detection. Subcritical cracking in the apparent absence of an environment in some materials is explained by 'atomistic' theories [41]. At 100 % RH calcite is much more susceptible to subcritical cracking [42].

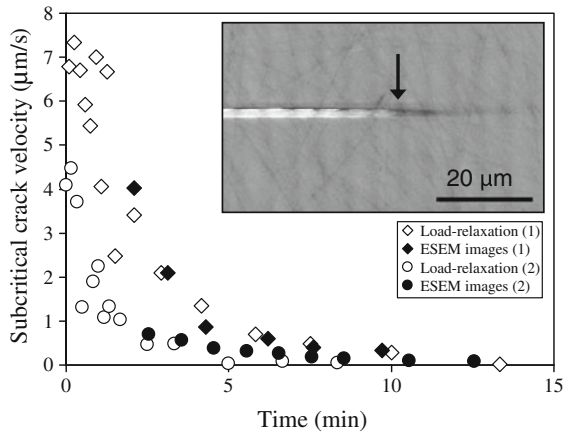

Fig. 3 Double torsion test results for calcite at 1 % RH and 25 °C

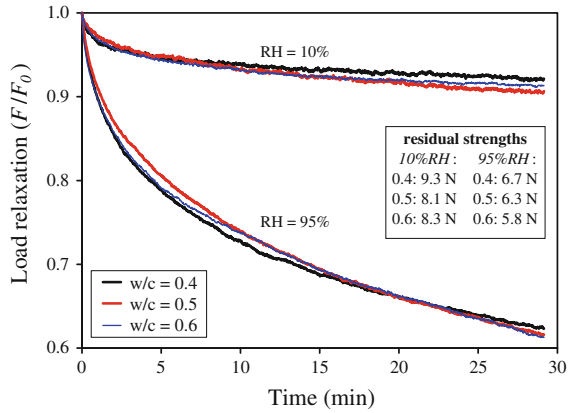

Fig. 4 Creep-induced load-relaxation of uncracked, unnotched 28 × 4 × 2 mm^3 specimens

3.2 Beam-bending tests

Cementitious materials exhibit significant creep at room temperature (as opposed to calcite) and this may cause load relaxation in the double torsion test in addition to subcritical crack propagation. In this study creep-induced load-relaxation as a function of w/c-ratio and relative humidity was measured using a beam-bending method on 28 × 4 × 2 mm^3 specimens without notch or guiding groove. The tests were run for 30 min, the same as the duration of the DT-tests. The results of cement pastes with w/c-ratio of 0.4, 0.5, and 0.6 and age of 9–10 months, equilibrated at 10 or 95 % RH at 20 °C are reported in Fig. 4. All specimens were loaded to 2.9 ± 0.1 N. The (residual) peak load upon reloading (P_{max}) of specimens equilibrated and tested at 10 % RH was 30–40 % higher than those equilibrated at 95 % RH (see table in Fig. 4). This means that the specific load-level (P/P_{max}) was 0.46 ± 0.02 and 0.34 ± 0.02 for the specimens at 10 and 95 % RH, respectively. The results show that cement pastes under the given conditions show significant creep-induced load-relaxation for the given specimen thickness of 2 mm, increasing with relative humidity. This is in agreement with earlier observations on the effect of relative humidity on creep [26–28]. In these experiments no significant effect of w/c-ratio on the relative load-relaxation in beam-bending was observed.

3.3 Traditionally calculated crack velocities

In order to compare our double torsion test results with those published earlier for cement paste [15–17], subcritical crack velocities and stress intensity factors were directly calculated using Eqs. 1 and 2 and plotted in the traditional *K*–*v* diagram (Fig. 5). Results for Portland cement pastes with added w/c-ratio's of 0.4, 0.5 and 0.6 at 10 or 90 % RH are shown. In our DT-tests, load-relaxation occurred due to subcritical crack growth as well as creep-induced load-relaxation (see further). The calculated crack velocities are thus overestimates. The position of the curves in the *K*–*v* diagram is first of all determined by the fracture toughness of the mixtures. For cement pastes the strength increases with the density of material which in turn is primarily determined by the w/c-ratio. For a given moisture content (10 or 90 %) the mixtures indeed increased in strength (i.e., *K*) with decreasing w/c-ratio.

With regard to subcritical cracking, the interpretation of the data in Fig. 5 is more complicated. In the case of glass, the importance of subcritical cracking increases with relative humidity of the environment [7]. The moisture diffuses to the crack tip in glass where it facilitates bond breaking by stress-corrosion [7]. When crack velocities are relatively low the rate of the stress-corrosion reaction determines the rate of subcritical cracking (region I cracking). The highest subcritical crack velocities are limited by the rate of diffusion of moisture to the crack tip, which causes a plateau in the *K*–*v* diagram, i.e., region II cracking [7]. Cement paste is a porous material with intrinsic moisture content depending on the environmental relative humidity [15]. In this study, the specimens were pre-equilibrated at the relative humidity of the environment. Thus, at for example 90 % RH,

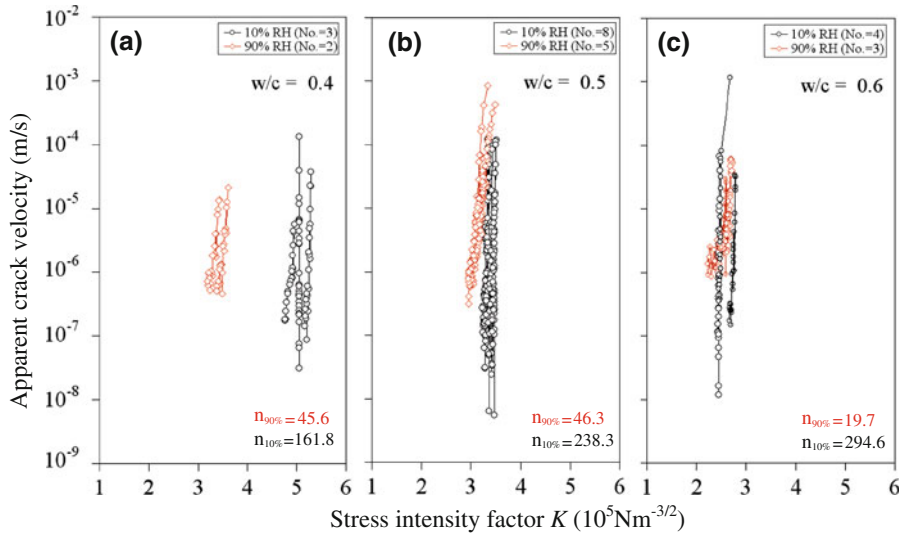

Fig. 5 Apparent subcritical crack velocities versus stress intensity factor calculated from load-relaxation measurements (Eqs. 1, 2). *n* represents the arithmetic mean value for the slopes of the *K*–*v* curves. Each *dot* in the diagram represents a single calculated value for *K* and *v*. No. means the number of measurements. The specimen thickness was 1.7 ± 0.05 mm

subcritical cracking may be caused by moisture that is already present in the capillary or gel pores of cement paste. Moisture diffusion from the environment to the crack tip is therefore expected to be less important than in glass and this could explain the absence of region II in the *K*–*v* diagram for cement paste [17, 43].

In cement paste it is expected that moisture not only affects subcritical cracking but also the fracture toughness or critical stress intensity factor (K_{IC}) as determined in fast loading experiments [23–25] and as suggested by the table in Fig. 4. According to Bažant and Prat [25] this may be caused by disjoining pressures of adsorbed water in the cement hydration products that lowers the fracture energy of the material. Thus, a shift of *K*–*v* curves to lower stress intensity factor values with increasing relative humidity may not only be due to subcritical cracking, but also partly because of the effect of moisture content on facture toughness.

Another measure for the susceptibility to subcritical cracking is the slope of the *K*–*v* curve (also called subcritical crack index), which is clearly lower for all mixtures at 90 % RH (Fig. 5). The slope is the *n*-value which is used in life-time analyses for making failure predictions for engineering materials [1, 14, 44]. However, if subcritical crack velocities are measured from the load-relaxation in DT-test and part of the load-relaxation is due to creep in the DT-specimens, then the *n*-values for subcritical cracking in the *K*–*v* diagram will be underestimated. In conclusion, the interpretation of traditional *K*–*v* diagrams for cement paste in terms of subcritical cracking needs to be done with caution.

3.4 Optically measured crack velocities

In this study double torsion tests were carried out in the ESEM or under the optical microscope to measure subcritical crack velocities optically. An example of subcritical cracking at 90 % RH is shown in Fig. 6 at low magnification under the optical stereomicroscope. It is evident that the crack tip propagation, as optically recorded in this example, does not correlate with the measured load-relaxation. The crack tip stopped propagating after 870 s, but the load-relaxation of the specimen continued. Also the crack opening, given as the crack opening strain (COS), decreased after 870 s (Fig. 6). Note that a COS of 0.1 corresponds to a crack opening of approximately 0.6 μm in this test. The specimen relaxation measured after 870 s was thus likely caused by specimen creep and not by subcritical cracking.

In all load-relaxation tests carried out at 10 % RH in the ESEM, the propagation or absence of propagation of the crack tip could be optically recorded at high magnification, in most cases facilitated by the use of DIC. In about 60 relaxation tests at 10 % RH, subcritical cracking stopped within the first 5 min of the test (Fig. 7a). In the first minute of a relaxation test only one or two images could be taken, because the crack tip usually moved out of the initial image frame after starting the relaxation test and therefore needed

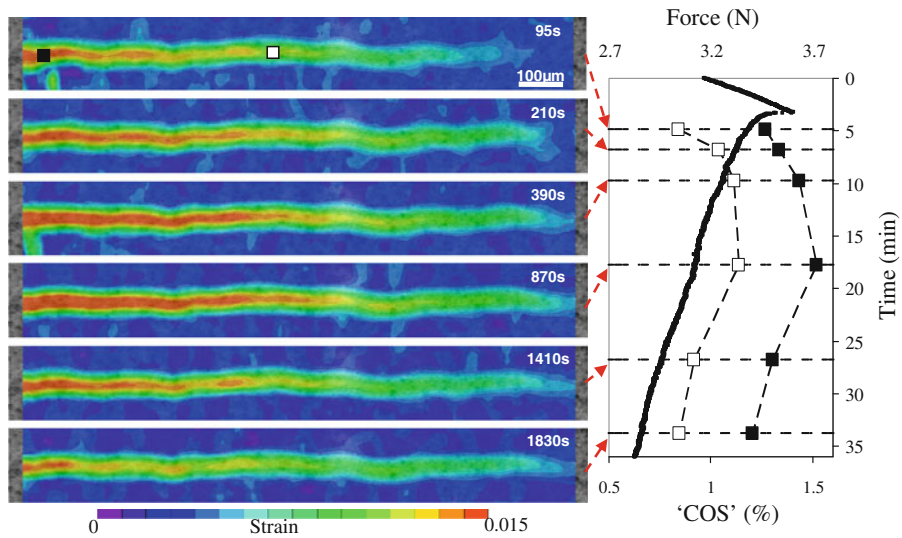

Fig. 6 (Color online). Digital image correlation (total principal tensile strain field) of subcritical crack growth (*left*) and measured load relaxation (*solid line* in diagram) from one double-torsion test under optical microscope at 90 % RH. *Filled* and *open squares* show the crack opening strain (COS) at two locations along the crack as shown in the image after 95 s

to be relocated by moving the sample stage. Also, acquiring an ESEM image by line-scanning took about 10 s in this study. In all these tests, the measured specimen load-relaxation continued after 5 min. From the load-relaxations measured after 5 min, the expected crack tip propagations according to Eq. 1 were calculated and they ranged between 20 and 100 μm. Since crack tip localization in ESEM is accurate within a few micrometers, it is clear that the specimen load relaxation measured after 5 min in these tests was not caused by actual crack propagation but more likely by specimen creep. Crack-arrest by discontinuities in the microstructure, such as unhydrated cement grains or portlandite crystals, could be responsible for this behavior.

In 20 different relaxation tests at 10 % RH we made 23 optical measurements of non-zero subcritical crack velocities. These velocities were compared with the average velocities calculated from the load-relaxation curve in the same test over the same time span. The ratio between these two velocities (v_{opt}/v_r) is plotted in Fig. 7b. The optically measured crack velocities for cement paste specimens at 10 % RH are with no exception smaller than those calculated from the load-relaxation curves. The ratio v_{opt}/v_r appears to go down with increasing time, suggesting that the relative contribution of creep in the DT-tests increased with time. For comparison the results for subcritical cracking in calcite are plotted, showing that the ratio v_{opt}/v_r is clearly closer to unity as expected for a non-creeping material.

A typical example of a subcritical crack propagating at 10 % RH during an ESEM DT-test is shown in Fig. 8. The crack tip position can be clearly identified with the help of DIC analysis. It can be seen that from 336 s till 456 s the crack tip stayed within the same image frame and propagated over a distance of about 20 μm. Then between 456 s and 700 s (Fig. 8b, c), the crack growth rate increased and after 1,000 s the crack had grown over a distance of about 330 μm to the position in Fig. 8d. No crack tip propagation was recorded after 1,000 s. This series of images shows that subcritical crack growth occurred in a discontinuous manner in hardened cement paste at low relative humidity. This is expected because the microstructure of cement paste is highly heterogeneous, thus the susceptibility to subcritical cracking is expected to vary from location to location. Note that recorded specimen load relaxation does not show any clear jumps associated with the discontinuous crack propagation observed at the specimen surface (Fig. 8). This is to be expected because in the DT-test the relaxation due to crack propagation over the specimen thickness is recorded, and as mentioned before, specimen creep contributes to the measured relaxation.

The subcritical crack index n from the K–v diagram can be used for life-time prediction for the material of interest [45]. If subcritical crack velocities are lower in reality than those calculated from DT-tests, and if this effect increases with time in the DT-test (see Fig. 7b), then the slopes of the

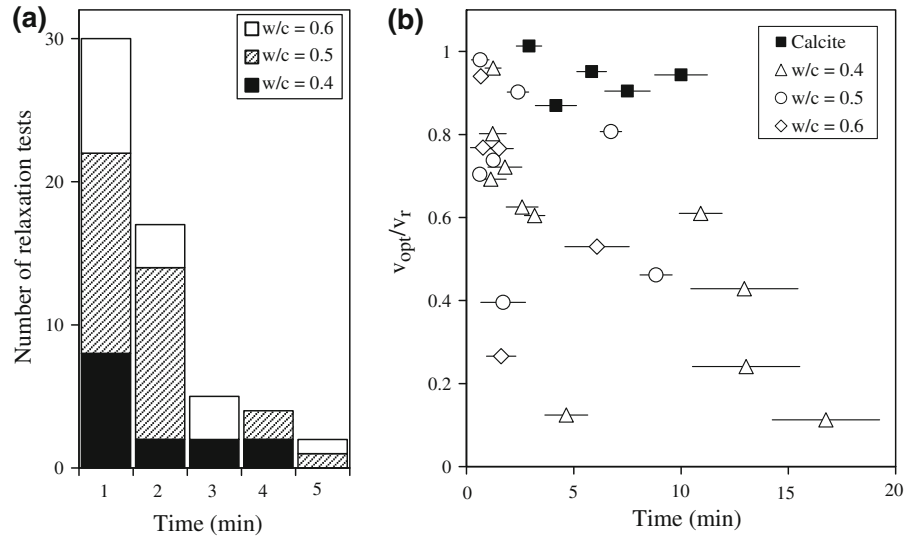

Fig. 7 **a** 58 relaxation tests at 10 % RH without notable subcritical cracking. The time refers to the time after which no distinguishable crack tip propagation was observed, which in most cases is when the second image was taken for the same location. **b** Ratio of optical and load-relaxation crack velocities (v_{opt}/v_r) as function of time in double-torsion tests at 10 % RH. *Horizontal error bars* indicate the time range used to calculate the velocity

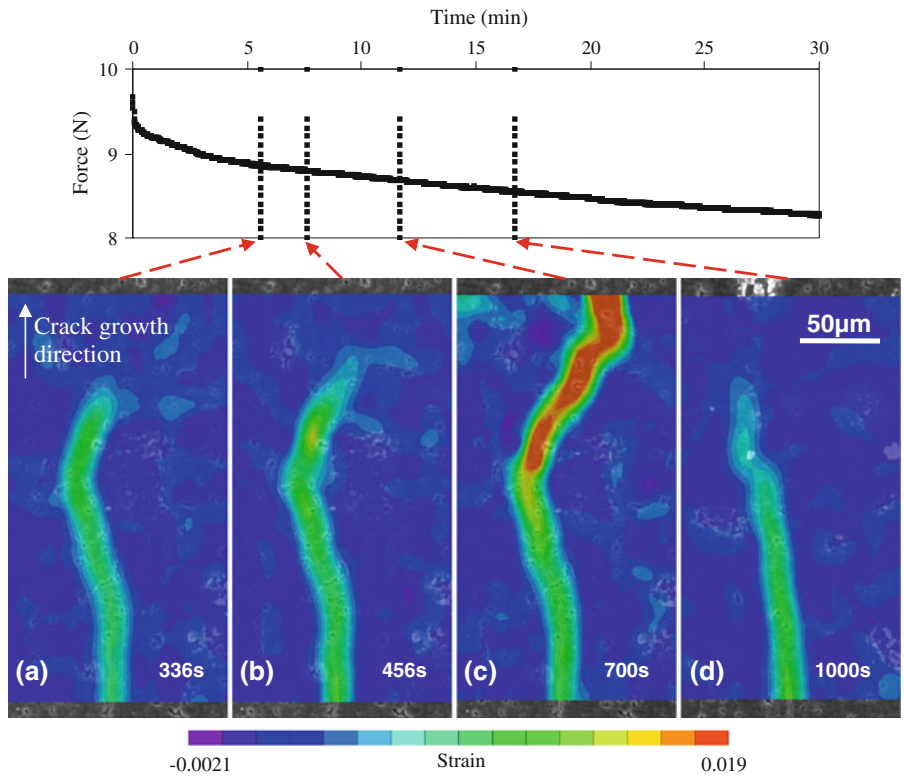

Fig. 8 Subcritical crack growth in cement paste in a DT-test inside the ESEM at 10 % RH (w/c-ratio = 0.4). The images are incremental principal strain fields obtained by DIC processing. **a**, **b** and **c** are for the same location. **d** is for the next crack tip location

traditional *K*–*v* diagram will give *n*-values that are too low. New experiments are underway to increase the success rate of optically measuring subcritical crack growth to obtain creep-free *n*-values for cement paste under practical moisture conditions of 50–100 % RH.

4 Conclusions

- The DT-specimens used in this study showed significant creep deformations. Subcritical crack velocities calculated from specimen load relaxation are overestimates in that case, and this will result in an underestimation of subcritical cracking index (n-value). Optically measured subcritical crack velocities could therefore provide a better basis for life-time analyses of cementitious materials under sustained loads.
- Digital image correlation is an effective tool to detect subcritical cracks in cementitious materials from ESEM or optical microscope images. In ESEM the maximum measurable crack velocity depends on image acquisition and sample stage movement rate and is in the practical range of 0.1–1 mm/s.
- Subcritical cracks in cementitious materials move in a step-wise manner and slowly propagating cracks are easily arrested in the DT-test by discontinuities in the microstructure. Subcritical cracking in cement paste stopped within minutes in most DT-tests at 10 % RH. At 90 % RH the susceptibility of cement paste to subcritical cracking appears to be much larger.

Acknowledgments We thank Mariano Pauli, Ernst Bleiker, Heinz Richner, Gabriele Peschke, Carsten Rieger, Dominik Meyer, Robert Flatt for their assistance in this project. This project was financed by the Swiss National Science Foundation (SNF), project nr. 200021-119787.

References

1. Mindess S (1985) Rate of loading effects on the fracture of cementitious materials. In: Shah SP (ed) Application of fracture mechanics to cementitious composites. Martinus Nijhoff, The Netherlands, pp 617–638
2. Wittmann FH (1985) Influence of time on crack formation and failure of concrete. In: Shah SP (ed) Application of fracture mechanics to cementitious composites. Martinus Nijhoff, The Netherlands, pp 593–616
3. Bažant ZP, Gettu R (1992) Rate effects of and load relaxation in static fracture of concrete. ACI Mat J 89:456–468
4. Bažant ZP, Xiang Y (1997) Crack growth and lifetime of concrete under long time loading. J Eng Mech 123:350–358
5. Van Zijl GPAG, De Borst R, Rots JG (2001) The role of crack rate dependence in the long-term behaviour of cementitious materials. Int J Solids Struct 38:5063–5079
6. Bažant ZP, Gu WH, Faber KT (1995) Softening reversal and other effect of a change in loading rate on fracture of concrete. ACI Mater J 92:3–9
7. Wiederhorn SM, Freiman SW, Fuller ER, Simmons CJ (1982) Effects of water and other dielectrics on crack growth. J Mater Sci 17:3460–3478
8. Freiman SW (1984) Effect of chemical environments on slow crack-growth in glasses and ceramics. J Geophys Res 89(NB6):4072–4076
9. Atkinson BK (1984) Subcritical crack growth in geological materials. J Geophys Res 89(B6):4077–4114
10. Stöckl S (1967) Tastversuche über den Einfluss von vorangegangen Dauerlasten auf die Kurzzeitfestigkeit des Betons, Deutscher Ausschuss für Stahlbeton No. 196:1–27
11. Shah SP, Chandra S (1970) Fracture of concrete subjected to cyclic and sustained loading. J Am Concr I 67:816–825
12. Hughes BP, Ash JE (1970) Some factors influencing the long-term strength of concrete. Mater Struct 3:81–84
13. Coutinho AS (1977) A contribution to the mechanism of concrete creep. Mater Struct 1:3–16
14. Nadeau JS, Mindess S, Hay JM (1974) Slow crack growth in cement paste. J Am Ceram Soc 57:51–54
15. Mindess S, Nadeau JS, Hay JM (1974) Effect of different curing conditions on slow crack growth in cement paste. Cem Concr Res 4:953–965
16. Evans AG, Clifton JR, Anderson E (1976) The fracture mechanics of mortars. Cem Concr Res 6:535–548
17. Beaudoin JJ (1985) Effect of humidity on subcritical crack growth in cement paste. Cem Concr Res 15:871–878
18. Beaudoin JJ (1985) Effect of water and other dielectrics on subcritical crack growth in Portland cement paste. Cem Concr Res 15:988–994
19. Denarié E, Cécot C, Huet C (2006) Characterization of creep and crack growth interactions in the fracture behaviour of concrete. Cem Concr Res 36:571–575
20. Wecharatana M, Shah SP (1980) Double torsion tests for studying slow crack-growth of Portland cement mortar. Cem Concr Res 10:833–844
21. Husak AD, Krokosky EM (1971) Static fatigue of hydrated cement concrete. J Am Concr I 68:263–271
22. Barrick JE, Krokosky EM (1976) The effects of temperature and relative humidity on static strength of hydrated Portland cement. J Test Eval 4:61–73
23. Beaudoin JJ (1982) Effect of humidity and porosity on fracture of hardened Portland cement. Cem Concr Res 12:705–716
24. Rossi P, Boulay C (1990) Influence of free water in concrete on the cracking process. Mag Concr Res 42:143–146
25. Bažant ZP, Prat PC (1999) Effect of temperature and humidity on fracture energy of concrete. ACI Mater J 85:262–271
26. Wittmann FH (1970) Einfluss des Feuchtigkeitsgehaltes auf das Kriechen des Zemensteins. Rhelo Acta 9:282–287
27. Bažant ZP, Asghari AA, Schmidt J (1976) Experimental study of creep of hardened Portland cement paste at variable water content. Mater Struct 9:279–290
28. Neville AM, Dilger WH, Brooks JJ (1983) Creep of plain and structural concrete. Construction Press, London, New York, p 361
29. Mindess S, Diamond S (1980) A preliminary SEM study of crack propagation in mortar. Cem Concr Res 10:509–519

30. Mindess S, Diamond S (1982) A device for direct observation of cracking of cement paste or mortar under compressive loading within a scanning electron microscope. Cem Concr Res 12:569–576
31. Diamond S, Mindess S, Lovell J (1983) Use of a Robinson backscatter detector and "wet cell" for examination of wet cement paste and mortar specimens under load. Cem Concr Res 13:107–113
32. Diamond S, Bentur A (1985) On the cracking in concrete and fiber-reinforced cements. In: Shah SP (ed) Application of fracture mechanics to cementitious composites. Martinus Nijhoff, The Netherlands, pp 87–140
33. Tait RB, Garrett GG (1986) In situ double torsion fracture studies of cement mortar and cement paste inside a scanning electron microscope. Cem Concr Res 16:143–155
34. Williams DP, Evans AG (1973) A simple method for studying slow crack growth. J Test Eval 1:264–270
35. Bažant ZP, Raftshol WJ (1982) Effect of cracking in drying and shrinkage specimens. Cem Concr Res 12:209–226
36. Bisschop J, Wittel F (2010) Contraction gradient induced microcracking in hardened cement paste. Cem Concr Comp. doi:10.1016/j.cemconcomp.2011.02.004
37. Fuller ER (1979) An evaluation of double-torsion testing-analysis. Fract Mech Appl Brittle Mater: 3–18
38. Choi S, Shah SP (1997) Measurement of deformations on concrete subjected to compression using image correlation. Exp Mech 37:307–313
39. Hild F, Roux S (2006) Digital image correlation: from displacement measurement to identification of elastic properties: a review. Strain 42:69–80
40. Bažant ZP, Bai SP, Gettu R (1993) Fracture of rock: effect of loading rate. Eng Fract Mech 45:393–398
41. Atkinson BK, Meredith PG (1987) The theory of subcritical crack growth with applications to minerals and rocks. In: Atkinson BK (ed) Fracture mechanics of rock. Academic Press, London
42. Røyne A, Bisschop J, Dysthe DK (2011) Experimental investigation of surface energy and subcritical crack growth in calcite. J Geoph Res B-Solid Earth. doi:10.1029/2010JB008033
43. Shyam A, Lara-Curzio A (2006) The double-torsion testing technique for determination of fracture toughness and slow crack growth behavior of materials: a review. J Mater Sci 41:4093–4104
44. Evans AG, Wiederhorn SM (1984) Proof testing of ceramic materials: an analytical basis for failure prediction. Int J Fract 26:355–368
45. Evans AG (1973) A simple method for evaluating slow crack growth in brittle materials. Int J Fract 9:267–275